Physics Letters B 745 (2015) 73–78

Contents lists available at ScienceDirect

Physics Letters B

www.elsevier.com/locate/physletb

Neutron skin and centrality classification in high-energy heavy-ion collisions at the LHC

Hannu Paukkunen [a,b,*]

[a] Department of Physics, University of Jyväskylä, P.O. Box 35, FI-40014 University of Jyväskylä, Finland
[b] Helsinki Institute of Physics, P.O. Box 64, FI-00014 University of Helsinki, Finland

ARTICLE INFO

Article history:
Received 11 March 2015
Received in revised form 17 April 2015
Accepted 18 April 2015
Available online 22 April 2015
Editor: J.-P. Blaizot

ABSTRACT

The concept of centrality in high-energy nuclear collisions has recently become a subject of an active debate. In particular, the experimental methods to determine the centrality that have given reasonable results for many observables in high-energy lead–lead collisions at the LHC have led to surprising behavior in the case of proton–lead collisions. In this letter, we discuss the possibility to calibrate the experimental determination of centrality by asymmetries caused by mutually different spatial distributions of protons and neutrons inside the nuclei — a well-known phenomenon in nuclear physics known as the neutron-skin effect.

1. Introduction

In high-energy heavy-ion experiments [1,2] like those now performed at the Large Hadron Collider (LHC), the collisions are often categorized according to their centrality aiming to separate the central head-on collisions from the peripheral ones in which only the edges of the nuclei collide. This has been generally realized by sorting the events according to the amount of particles or energy deposited in specific parts of the detector, details varying from one experiment to another [3–6]. In its simplicity, the idea is that in increasingly central collisions the colliding nuclei disintegrate more completely thereby producing more particles. In nucleus–nucleus collisions, an existence of a correspondence between the intuitive geometrical notion of centrality and its experimental determination is supported by the systematics of azimuthal anisotropies [7,8] in the spectra of low-transverse-momentum (low-p_T) particles [6,9–11] which, in models based on classical collective dynamics [12–14] are readily interpreted as reflecting the initial geometry of the collision zone.

Similar experimental procedures in proton–nucleus collisions at the LHC have revealed much stronger centrality dependence of hard-process observables, like high-p_T jets [15,16], than what was anticipated e.g. from models for impact-parameter dependent nuclear effects in parton distribution functions (PDFs) [17,18]. At the same time, however, the minimum-bias versions of the same jet observables — obtained by "integrating out" the variable used for the centrality classification — are in good agreement [15,16,19] with the predictions based on collinearly factorized Quantum Chromo-Dynamics (QCD). This appears to indicate that the current experimental methods to realize the centrality classification seriously interfere [20,21] with the hard processes and, among other proposals [22–25], it has been argued [26] that even the standard energy–momentum conservation plays a significant role. On top of this, the presence of event-by-event fluctuations in the initial profile of nucleons inside nucleus can further distort the multiplicity-based experimental centrality classification. In the aggregate, the way that the centrality-selected measurements in proton–nucleus collisions should be interpreted has turned out largely ambiguous. In nucleus–nucleus collisions interferences between the hard processes and the centrality categorization are of less importance as the multiplicity of low-p_T particles used in the events' centrality classification is much larger and the correlations get diluted.

In this letter, we will discuss a centrality-dependent effect (in its geometric meaning) which stems from the fact that in spherical, neutron-rich nuclei the concentration of neutrons is known to increase towards the nuclear surface [27,28]. We demonstrate how this causes effects in electroweak processes that should be large enough to be measured at the LHC and could thereby help in resolving open issues concerning the relationship between theoretical concept of centrality and its experimental counterpart.

* Correspondence to: Department of Physics, University of Jyväskylä, P.O. Box 35, FI-40014 University of Jyväskylä, Finland.
E-mail address: hannu.paukkunen@jyu.fi.

http://dx.doi.org/10.1016/j.physletb.2015.04.037

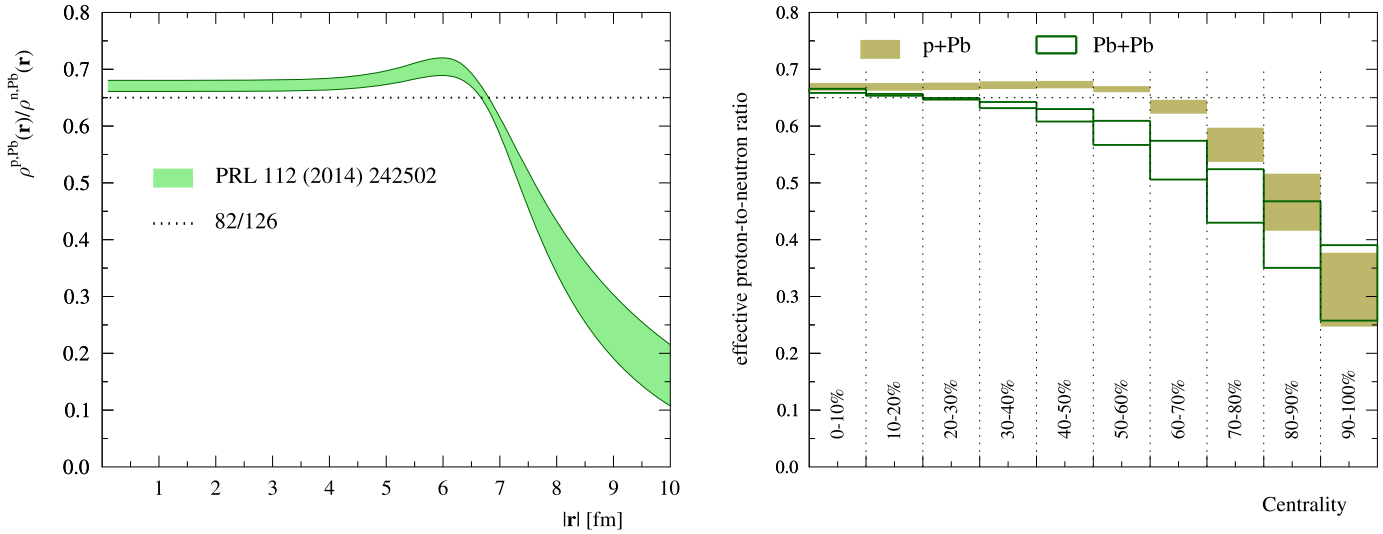

Fig. 1. Left-hand panel: The measured ratio of proton and neutron densities in ^{208}Pb as a function of nuclear radius. Right-hand panel: The ratio $Z_{\rm eff}(\mathcal{C}_k)/N_{\rm eff}(\mathcal{C}_k)$ for different centrality classes in p + Pb (filled yellow rectangles) and Pb + Pb collisions (open green rectangles). The heights of the rectangles are determined by the uncertainties given for the neutron density in Ref. [27].

2. Collision geometry and Glauber modeling

The density of nucleons i in a spherical nucleus A is often parametrized using the two-parameter Fermi (2pF) distribution as

$$\rho^{i,A}(\mathbf{r}) = \rho_0^{i,A}/(1+e^{\frac{|\mathbf{r}|-d_i}{a_i}}), \tag{1}$$

where the half-density parameter d_i controls size of the nuclear core and a_i the thickness of the nuclear surface. The saturation densities $\rho_0^{i,A}$ are determined by requiring the total amount of protons and neutrons to remain constant (we consider only ^{208}Pb nucleus in this paper),

$$\int d^3\mathbf{r}\rho^{\rm p,A}(\mathbf{r}) = Z = 82, \qquad \int d^3\mathbf{r}\rho^{\rm n,A}(\mathbf{r}) = N = 126. \tag{2}$$

It is an experimental fact [27,28] that in neutron-rich spherical nuclei the relative amount of neutrons in comparison to protons increases near the surface of the nucleus. This is usually referred to as neutron-skin effect: In short, the Coulomb barrier that builds up from the positively charged protons limits the extent that the proton density can stretch out whereas, being blind to the Coulomb interaction, the neutrons can be found further away [29]. The most recent measurement of this phenomenon [27] for ^{208}Pb nucleus indicates that the neutron skin does not, unlike its name suggests, have a sharp edge but rather a "halo-like" character. As shown in the left-hand panel of Fig. 1, the proton-to-neutron ratio, $\rho^{\rm p,A}/\rho^{\rm n,A}$, does not drop abruptly but the fall-off towards the edge of the nucleus is gradual. In this plot (and throughout the rest of this paper) we have used the parameter values $a_{\rm p} = 0.447$ fm, $d_{\rm p} = 6.680$ fm for protons, and $a_{\rm n} = 0.55 \pm 0.03$ fm, $d_{\rm n} = 6.70 \pm 0.03$ fm for neutrons, taken from Ref. [27], and the error band results from adding the variations caused by the quoted two uncertainties in quadrature.

The Optical Glauber Model [30] is a commonly used tool in heavy-ion collisions [31–33]. In this approach, the total inelastic cross section $\sigma_{AB}^{\rm inel}(s)$ in collisions of two nuclei A and B with certain center-of-mass energy $\sqrt{s}$ is given by the integral

$$\sigma_{AB}^{\rm inel}(s) = \int_{-\infty}^{\infty} d^2\mathbf{b}\left[1 - e^{-T_{AB}(\mathbf{b})\,\sigma^{\rm inel}(s)}\right], \tag{3}$$

where $\mathbf{b}$ is the vector between the centers of the colliding nuclei in transverse plane (see e.g. Fig. 20 in Ref. [17]), $\sigma^{\rm inel}(s)$ is the inelastic nucleon–nucleon cross section,[1] and $T_{AB}(\mathbf{b})$ is the nuclear overlap function

$$T_{AB}(\mathbf{b}) \equiv \int_{-\infty}^{\infty} d^2\mathbf{s}\left[T_A^{\rm p}(\mathbf{s}_1) + T_A^{\rm n}(\mathbf{s}_1)\right]\left[T_B^{\rm p}(\mathbf{s}_2) + T_B^{\rm n}(\mathbf{s}_2)\right], \tag{4}$$

with $\mathbf{s}_{1,2} \equiv \mathbf{s} \pm \mathbf{b}/2$, and

$$T_A^i(\mathbf{r}) \equiv \int_{-\infty}^{\infty} dz\rho^{\rm i,A}(\mathbf{r}, z). \tag{5}$$

The centrality classes $\mathcal{C}_k$ are defined as ordered impact-parameter intervals $b_k \le |\mathbf{b}| \le b_{k+1}$, such that a certain percentage $(c_{k+1} - c_k)\%$ of the total inelastic cross section accumulates upon integrating,

$$(c_{k+1} - c_k)\% = \frac{1}{\sigma_{AB}^{\rm inel}} \int_{-\infty}^{\infty} d^2\mathbf{b}\left[1 - e^{-T_{AB}(\mathbf{b})\,\sigma^{\rm inel}}\right] \times \theta\big(b_{k+1} - |\mathbf{b}|\big)\theta\big(|\mathbf{b}| - b_k\big). \tag{6}$$

Let us now consider a given hard process (e.g. large-p_T direct photon production or equivalent) whose contribution to $\sigma^{\rm inel}$ is negligible and does thereby not "interfere" with our centrality categorization. We write the cross section for such a process within a given centrality class $\mathcal{C}_k$ as

$$d\sigma_{AB}^{\rm hard}(\mathcal{C}_k) = 2\pi \int_{b_k}^{b_{k+1}} dbb \int_{-\infty}^{\infty} d^2\mathbf{s} \times \sum_{i,j} T_A^i(\mathbf{s}_1) T_B^j(\mathbf{s}_2) d\sigma_{ij}^{\rm hard}(A, B, \mathbf{s}_1, \mathbf{s}_2), \tag{7}$$

[1] The total inelastic cross section should be isospin symmetric as it does not separate the particles of different charge. That is, we assume $\sigma^{\rm inel} = \sigma_{\rm pp}^{\rm inel} = \sigma_{\rm nn}^{\rm inel} = \sigma_{\rm pn}^{\rm inel} = \sigma_{\rm np}^{\rm inel}$.

where the sum runs over different combinations of protons and neutrons. The nucleon–nucleon hard-process cross sections $d\sigma_{ij}^{\mathrm{hard}}(A, B, \mathbf{s}_1, \mathbf{s}_2)$ can, in general, depend on the size of the nuclei (via nuclear shadowing or equivalent [34–36]) and even on the spatial location of the nucleons inside the nuclei [37,17]. However, to underscore the neutron-vs-proton differences alone we assume here that such effects are approximately constant within each centrality class and write the above cross section as

$$d\sigma_{AB}^{\mathrm{hard}}(\mathcal{C}_k) = \langle nn\rangle_{\mathcal{C}_k} d\sigma_{\mathrm{nn}}^{\mathrm{hard}}(\mathcal{C}_k) + \langle pp\rangle_{\mathcal{C}_k} d\sigma_{\mathrm{pp}}^{\mathrm{hard}}(\mathcal{C}_k) + \langle np\rangle_{\mathcal{C}_k} d\sigma_{\mathrm{np}}^{\mathrm{hard}}(\mathcal{C}_k) + \langle pn\rangle_{\mathcal{C}_k} d\sigma_{\mathrm{pn}}^{\mathrm{hard}}(\mathcal{C}_k), \tag{8}$$

where

$$\langle ij\rangle_{\mathcal{C}_k} \equiv 2\pi \int_{b_k}^{b_k+1} dbb \int_{-\infty}^{\infty} d^2\mathbf{s} T_A^{\mathrm{i}}(\mathbf{s}_1) T_B^{\mathrm{j}}(\mathbf{s}_2), \tag{9}$$

and $d\sigma_{ij}^{\mathrm{hard}}(\mathcal{C}_k)$ refer to nucleon–nucleon cross sections in a given centrality class. It turns out that for symmetric A+A collisions (for the centrality categories considered here),

$$\langle np\rangle_{\mathcal{C}_k} = \langle pn\rangle_{\mathcal{C}_k} \approx \sqrt{\langle pp\rangle_{\mathcal{C}_k}\langle nn\rangle_{\mathcal{C}_k}}, \tag{10}$$

and we can visualize a given centrality class $\mathcal{C}_k$ as simply containing events from collisions of two nuclei with effective number of protons $Z_{\mathrm{eff}}^{AA}(\mathcal{C}_k)$ and neutrons $N_{\mathrm{eff}}^{AA}(\mathcal{C}_k)$ defined as

$$Z_{\mathrm{eff}}^{\mathrm{AA}}(\mathcal{C}_k) \equiv \sqrt{\langle pp\rangle_{\mathcal{C}_k}}\,, \quad N_{\mathrm{eff}}^{\mathrm{AA}}(\mathcal{C}_k) \equiv \sqrt{\langle nn\rangle_{\mathcal{C}_k}}\,. \tag{11}$$

The case of proton–nucleus collisions can be obtained by replacing the 2pF-distribution for the projectile proton by a delta function $\rho^p = \delta^{(3)}(\mathbf{r})$. As a result, the hard-scattering cross section becomes

$$d\sigma_{pA}^{\mathrm{hard}}(\mathcal{C}_k) = \langle p\rangle_{\mathcal{C}_k} d\sigma_{\mathrm{pp}}^{\mathrm{hard}}(\mathcal{C}_k) + \langle n\rangle_{\mathcal{C}_k} d\sigma_{\mathrm{pn}}^{\mathrm{hard}}(\mathcal{C}_k), \tag{12}$$

with

$$\langle i\rangle_{\mathcal{C}_k} \equiv 2\pi \int_{b_k}^{b_k+1} dbb T_A^{\mathrm{i}}(\mathbf{b}), \tag{13}$$

and the effective nucleus which the projectile proton "sees" consists of

$$Z_{\mathrm{eff}}^{\mathrm{pA}}(\mathcal{C}_k) \equiv \langle p\rangle_{\mathcal{C}_k}\,, \quad N_{\mathrm{eff}}^{\mathrm{pA}}(\mathcal{C}_k) \equiv \langle n\rangle_{\mathcal{C}_k}\,, \tag{14}$$

protons and neutrons, respectively. To evaluate the effective number of nucleons in each case, we have used $\sigma^{\mathrm{inel}}(\sqrt{s} = 2.76\ \mathrm{TeV}) = 65$ mb (for Pb + Pb), and $\sigma^{\mathrm{inel}}(\sqrt{s} = 5.02\ \mathrm{TeV}) = 70$ mb (for p + Pb) for the inelastic nucleon–nucleon cross sections [38]. The resulting effective proton-to-neutron ratios $Z_{\mathrm{eff}}^{\mathrm{pPb}}(\mathcal{C}_k)/N_{\mathrm{eff}}^{\mathrm{pPb}}(\mathcal{C}_k)$ and $Z_{\mathrm{eff}}^{\mathrm{PbPb}}(\mathcal{C}_k)/N_{\mathrm{eff}}^{\mathrm{PbPb}}(\mathcal{C}_k)$ computed using Eqs. (11) and (14) in various centrality classes are shown in the right-hand panel of Fig. 1. While in most central collisions these ratios are very close to the average value $Z/N = 82/126 \approx 0.65$, in very peripheral bins the relative amount of neutrons grows. Since the edges of the nuclei are always inside the integration domain in Eq. (9), the effect of neutron skin in lead–lead starts to be visible in more central collision than in the case of proton–lead. This observation also hints that our assumption of a point-like proton makes the centrality-dependent effects slightly weaker than what would be obtained by assigning the proton with a finite size.

3. Effects of neutron skin in $W^{\pm}$ production

To make the variations in proton-to-neutron ratio visible, an observable for which $d\sigma_{\mathrm{nn}}^{\mathrm{hard}} \neq d\sigma_{\mathrm{pp}}^{\mathrm{hard}} \neq d\sigma_{\mathrm{pn}}^{\mathrm{hard}}$ is required. As the only significant difference[2] between the protons and neutrons is their u and d valence-quark content, we need a probe which couples differently to u and d flavors. Here, we will consider the production of inclusive charged leptons $\ell^{\pm}$ from $W^{\pm} \to \ell^{\pm}\nu$ decays. This process is theoretically particularly well understood, the collinearly factorized perturbative QCD calculations known up to next-to-next-to-leading order [41,42], and the state-of-the-art calculations incorporate also next-to-leading order electroweak corrections [43] on top of this. The existing minimum bias LHC measurements for this process in proton–lead and lead–lead collisions are roughly consistent with the pQCD predictions [44–46].

In the narrow-width approximation, accurate in the asymptotic limit when the decay width Γ_{W} of the $\mathrm{W}^{\pm}$ boson is much less than its mass M_{W}, the leading-order expressions [47,48] for the charged-lepton rapidity (y) and transverse momentum (p_T) distribution can be cast as

$$\begin{aligned}\frac{d\sigma^{\ell^{\mp}}}{dydp_T} \approx{}& \frac{\pi^2}{24s}\left(\frac{\alpha_{\mathrm{em}}}{\sin^2\theta_{\mathrm{W}}}\right)^2 \frac{1}{M_{\mathrm{W}}\Gamma_{\mathrm{W}}} \frac{p_T}{\sqrt{1-4p_T^2/M_{\mathrm{W}}^2}} \\ &\times \sum_{i,j} |V_{ij}|^2\, \delta\left(e_{q_i} + e_{\bar{q}_j} \pm 1\right) \\ &\times \Big\{\alpha^{\pm}\Big[f_{q_i}^{\mathrm{A}}(\xi_1^+, Q^2) f_{\bar{q}_j}^{\mathrm{B}}(\xi_2^+, Q^2) \\ &+ f_{\bar{q}_j}^{\mathrm{A}}(\xi_1^-, Q^2) f_{q_i}^{\mathrm{B}}(\xi_2^-, Q^2)\Big] \\ &+ \alpha^{\mp}\Big[f_{q_i}^{\mathrm{A}}(\xi_1^-, Q^2) f_{\bar{q}_j}^{\mathrm{B}}(\xi_2^-, Q^2) \\ &+ f_{\bar{q}_j}^{\mathrm{A}}(\xi_1^+, Q^2) f_{q_i}^{\mathrm{B}}(\xi_2^+, Q^2)\Big]\Big\}\end{aligned} \tag{15}$$

where $\alpha^{\pm} = 1 \pm (1 - 4p_T^2/M_{\mathrm{W}}^2)^{1/2}$, and the symbols α_{em}, θ_{W} and V_{ij} denote the fine-structure constant, weak-mixing angle and Cabibbo–Kobayashi–Maskawa matrix, respectively. The sum over all partonic flavors is restricted by the δ function which selects only those combinations of quarks and antiquarks for which the electric charges e_{q_i}, $e_{\bar{q}_j}$ sum up correctly to the charge of the lepton. The momentum arguments of the PDFs for quarks $f_{q_i}^{\mathrm{A}}(x, Q^2)$ and antiquarks $f_{\bar{q}_i}^{\mathrm{A}}(x, Q^2)$ are given by

$$\begin{aligned}\xi_1^{\pm} &\equiv \frac{M_{\mathrm{W}}^2 e^{y}}{2p_T\sqrt{s}}\left[1 \mp \sqrt{1 - 4p_T^2/M_{\mathrm{W}}^2}\right], \\ \xi_2^{\pm} &\equiv \frac{M_{\mathrm{W}}^2 e^{-y}}{2p_T\sqrt{s}}\left[1 \pm \sqrt{1 - 4p_T^2/M_{\mathrm{W}}^2}\right].\end{aligned} \tag{16}$$

To account for the centrality-dependence of the hard-scattering cross sections, we use PDFs $f_i^{\mathrm{Pb},\mathcal{C}_k}(x, Q^2)$ for the lead nucleus defined as

$$f_i^{\mathrm{Pb},\mathcal{C}_k}(x, Q^2) \equiv Z_{\mathrm{eff}}^{\mathrm{pPb,PbPb}}(\mathcal{C}_k) f_i^{\mathrm{p},\mathcal{C}_k}(x, Q^2) + N_{\mathrm{eff}}^{\mathrm{pPb,PbPb}}(\mathcal{C}_k) f_i^{\mathrm{n},\mathcal{C}_k}(x, Q^2), \tag{17}$$

where $f_i^{\mathrm{p},\mathcal{C}_k}$ and $f_i^{\mathrm{n},\mathcal{C}_k}$ are proton and neutron PDFs in a given centrality class $\mathcal{C}_k$, the latter obtained from the former based on the isospin symmetry (e.g. $f_u^{\mathrm{n},\mathcal{C}_k} = f_d^{\mathrm{p},\mathcal{C}_k}$). Other nuclear effects like

[2] We neglect the photon distribution [39,40].

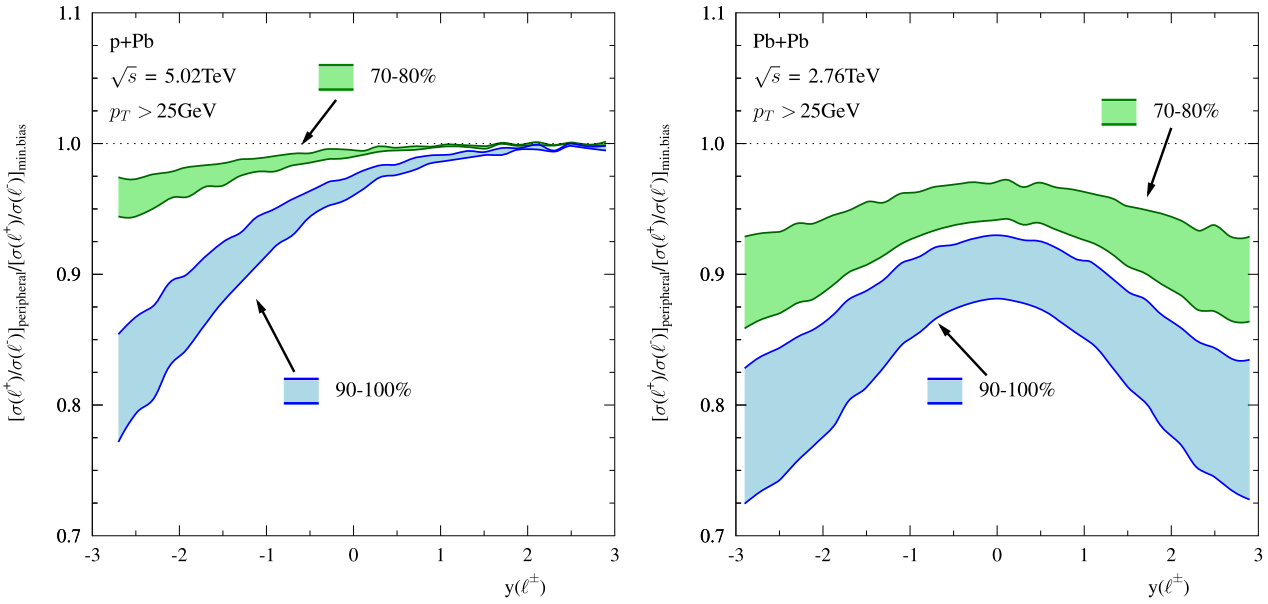

Fig. 2. Left-hand panel: The ratio $d\sigma^{\ell^+}/d\sigma^{\ell^-}$ in proton–lead collisions for two peripheral centrality class normalized by the corresponding ratio in the minimum bias collisions. Right-hand panel: As the left-hand panel, but for lead–lead collisions. The small wiggles are residual fluctuations from the Monte-Carlo integrations in MCFM.

shadowing can be incorporated as multiplicative correction factors $R_i^{\mathcal{C}_k}(\xi, Q^2)$ on the proton PDFs,

$$f_i^{\mathrm{p},\mathcal{C}_k}(\xi, Q^2) = R_i^{\mathcal{C}_k}(\xi, Q^2) f_i^{\mathrm{p}}(\xi, Q^2). \tag{18}$$

In the case of minimum bias collisions these correction factors and their uncertainties have been estimated in several global fits [49–52], and models for their possible centrality dependence exist [37,17]. However, in this letter, we will consider only ratios $d\sigma(\ell^+)/d\sigma(\ell^-)$ and nuclear modifications like this are expected to largely cancel even if they were centrality dependent: At a high factorization scale like $Q^2 \propto M_{\mathrm{W}}^2$ involved here, most of the sea quarks originate from collinear gluon splittings ($g \to q\bar{q}$) which is a flavor-independent process for light quarks. Furthermore, the mutually very similar nuclear effects observed in charged-lepton [34,36] and neutrino deep-inelastic scattering [53] on Pb nucleus indicate that the nuclear corrections for the valence quarks are also approximately equal, $R_{u_{\mathrm{v}}}^{\mathcal{C}_k}(\xi, Q^2) \approx R_{d_{\mathrm{v}}}^{\mathcal{C}_k}(\xi, Q^2)$. As a result, the overall nuclear corrections for ℓ^+ and ℓ^- production must be mutually very alike and largely cancel upon taking the ratio, separately in each centrality class. In fact, the results shown in plots below have been obtained by setting $f_i^{\mathrm{p},\mathcal{C}_k} = f_i^{\mathrm{p}}$ where f_i^{p} are free proton PDFs for which we have used the general-purpose CT10NLO parametrization [54]. Another attractive feature that the ratio $d\sigma(\ell^+)/d\sigma(\ell^-)$ entails is that many experimental systematic uncertainties can be expected to cancel out. Furthermore, one does not need an absolute normalization which would need further Glauber modeling.

The results that follow have been obtained by using the MCFM Monte-Carlo code [55,56] at next-to-leading order accuracy with the factorization and renormalization scales Q^2 fixed to M_{W}. To mimic a realistic experimental situation, we integrate over the charged lepton transverse momentum with $p_T > 25$ GeV.

3.1. Proton–lead collisions

The effect of the neutron skin will be most pronounced in the kinematic region where the large-x nuclear valence quarks $f_{u_{\mathrm{v}}}^{\mathrm{p},\mathcal{C}_k}(x)$ and $f_{d_{\mathrm{v}}}^{\mathrm{p},\mathcal{C}_k}(x)$ are of importance. From Eq. (16) we see that this happens towards negative values of y (the "backward" direction). The resulting centrality dependence of ratios $d\sigma(\ell^+)/d\sigma(\ell^-)$ in p + Pb collisions is illustrated in the left-hand panel of Fig. 2 by comparing two peripheral classes 70–80% and 90–100% to the minimum bias one, 0–100%. Since the main contributions to the cross sections come from the $u\bar{d}$ and $d\bar{u}$ partonic channels [57] and the sea-quark distributions at small x and large factorization scale $Q^2 = M_{\mathrm{W}}^2$ are approximately flavor independent, $f_{\bar{d}}^{\mathrm{p}}(x, Q^2) \approx f_{\bar{u}}^{\mathrm{p}}(x, Q^2)$, we can approximate

$$\frac{d\sigma^{\ell^+}_{\mathrm{p+Pb}}}{d\sigma^{\ell^-}_{\mathrm{p+Pb}}}\Big|_{y\ll 0} \approx \left(\frac{\alpha^-}{\alpha^+}\right) \times \frac{\left[Z_{\mathrm{eff}}^{\mathrm{pPb}}(\mathcal{C}_k)/N_{\mathrm{eff}}^{\mathrm{pPb}}(\mathcal{C}_k)\right] f_{u_{\mathrm{v}}}^{\mathrm{p},\mathcal{C}_k}(\xi_2^-, Q^2) + f_{d_{\mathrm{v}}}^{\mathrm{p},\mathcal{C}_k}(\xi_2^-, Q^2)}{\left[Z_{\mathrm{eff}}^{\mathrm{pPb}}(\mathcal{C}_k)/N_{\mathrm{eff}}^{\mathrm{pPb}}(\mathcal{C}_k)\right] f_{d_{\mathrm{v}}}^{\mathrm{p},\mathcal{C}_k}(\xi_2^-, Q^2) + f_{u_{\mathrm{v}}}^{\mathrm{p},\mathcal{C}_k}(\xi_2^-, Q^2)}. \tag{19}$$

As $f_{d_{\mathrm{v}}}^{\mathrm{p},\mathcal{C}_k}(x, Q^2)/f_{u_{\mathrm{v}}}^{\mathrm{p},\mathcal{C}_k}(x, Q^2) < 1$, the derivative of this expression with respect to $Z_{\mathrm{eff}}^{\mathrm{pPb}}(\mathcal{C}_k)/N_{\mathrm{eff}}^{\mathrm{pPb}}(\mathcal{C}_k)$ is positive and, in line with Fig. 2, the ratio $d\sigma^{\ell^+}/d\sigma^{\ell^-}$ decreases towards more peripheral collisions (since $Z_{\mathrm{eff}}^{\mathrm{pPb}}(\mathcal{C}_k)/N_{\mathrm{eff}}^{\mathrm{pPb}}(\mathcal{C}_k)$ decreases). Towards positive values of y (the "forward" direction), we have

$$\frac{d\sigma^{\ell^+}_{\mathrm{p+Pb}}}{d\sigma^{\ell^-}_{\mathrm{p+Pb}}}\Big|_{y\gg 0} \approx \left(\frac{\alpha^-}{\alpha^+}\right) \frac{f_{u_{\mathrm{v}}}^{\mathrm{p}}(\xi_1^+, Q^2)}{f_{d_{\mathrm{v}}}^{\mathrm{p}}(\xi_1^+, Q^2)}, \tag{20}$$

where we have assumed that the small-x sea quark distributions in Pb nucleus are approximately flavor independent at large Q^2, $f_{\bar{u}}^{\mathrm{Pb},\mathcal{C}_k}(x, Q^2) \approx f_{\bar{d}}^{\mathrm{Pb},\mathcal{C}_k}(x, Q^2)$. The independence of $Z_{\mathrm{eff}}^{\mathrm{pPb}}(\mathcal{C}_k)/N_{\mathrm{eff}}^{\mathrm{pPb}}(\mathcal{C}_k)$ explains why the centrality dependence of $d\sigma^{\ell^+}/d\sigma^{\ell^-}$ virtually disappears towards large values of y. Currently, no centrality classified proton–lead data for $W^\pm$ production are available.

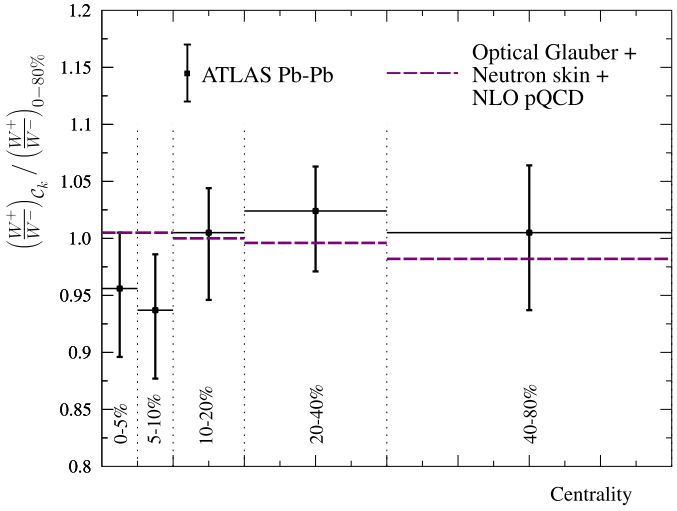

Fig. 3. The centrality dependence of W^+/W^- ratio as measured by ATLAS Collaboration [45] compared to the calculation presented in this paper. The reported experimental values of W^+/W^- ratio in each centrality class have been normalized to the average one $(W^+/W^-)_{0-80\%} = 1.03$ and the uncertainties have been obtained by adding in quadrature the statistical and systematic uncertainties.

3.2. Lead–lead collisions

The right-hand panel of Fig. 2 presents the results in the case of symmetric Pb + Pb collisions. As earlier, sufficiently far away from the midrapidity, $|y| \gg 0$, we can approximate

$$\frac{d\sigma^{\ell^+}_{\mathrm{Pb+Pb}}}{d\sigma^{\ell^-}_{\mathrm{Pb+Pb}}}\Big|_{|y|\gg 0} \approx \left(\frac{\alpha^-}{\alpha^+}\right) \frac{\left[Z^{\mathrm{PbPb}}_{\mathrm{eff}}(\mathcal{C}_k)/N^{\mathrm{PbPb}}_{\mathrm{eff}}(\mathcal{C}_k)\right] f^{\mathrm{p},\mathcal{C}_k}_{u_v}(x,Q^2) + f^{\mathrm{p},\mathcal{C}_k}_{d_v}(x,Q^2)}{\left[Z^{\mathrm{PbPb}}_{\mathrm{eff}}(\mathcal{C}_k)/N^{\mathrm{PbPb}}_{\mathrm{eff}}(\mathcal{C}_k)\right] f^{\mathrm{p},\mathcal{C}_k}_{d_v}(x,Q^2) + f^{\mathrm{p},\mathcal{C}_k}_{u_v}(x,Q^2)} \tag{21}$$

where now $x = \xi_2^-$ for $y \ll 0$, and $x = \xi_1^+$ for $y \gg 0$. Similarly as in the case of proton–lead, the dependence of $Z^{\mathrm{PbPb}}_{\mathrm{eff}}(\mathcal{C}_k)/N^{\mathrm{PbPb}}_{\mathrm{eff}}(\mathcal{C}_k)$ explains the stronger suppression of $d\sigma(\ell^+)/d\sigma(\ell^-)$ towards peripheral collisions. In comparison to the proton–lead collisions, the effect is better visible even at $y = 0$ since both the sea-valence and valence-sea scatterings depend on $Z^{\mathrm{PbPb}}_{\mathrm{eff}}(\mathcal{C}_k)/N^{\mathrm{PbPb}}_{\mathrm{eff}}(\mathcal{C}_k)$ while in proton–lead collisions this happens only for sea-valence contribution.

Currently, the most accurate experimental measurements of $W^\pm$ production in lead–lead collisions come from ATLAS Collaboration [45]. The data for W^+/W^- ratio are plotted in Fig. 3 and compared to the calculation described in this letter. The data, as well as the MCFM computation, include all $W^\pm$ events within the kinematic region restricted by the lepton transverse momentum $p_T > 25$ GeV, pseudorapidity interval $|\eta^{\ell^\pm}| < 2.5$, missing transverse momentum $p_T^{\mathrm{missing}} > 25$ GeV, and the transverse mass of the $\ell^\pm\nu$ system $m_T > 40$ GeV. While our calculation is consistent with the data, $\chi^2/N_{\mathrm{data}} \approx 0.6$ (N_{data} is the number of data points), the measurements are clearly not accurate enough and have a too coarse centrality categorization to draw conclusions to any direction at this stage.

4. Summary and outlook

We have discussed the generic effects that mutually different spatial distributions of protons and neutrons in heavy nuclei are expected to induce in production of $W^\pm$ bosons at the LHC. The proton density is known to fall off more rapidly than that of neutrons towards the surface of neutron-rich nuclei like ^{208}Pb which, as we have demonstrated, correlates with the sign of the produced $W^\pm$ boson. Thus, the $W^\pm$ production could be used to benchmark different experimental definitions of centrality at the LHC. We stress that in this paper we have considered the centrality from a purely geometric viewpoint neglecting e.g. possible smearing of the effect that could be caused by event-by-event fluctuations. Therefore, our results should be taken as first, rough estimates of the expected systematics if a given experimental centrality-selection method truly reflects the collision geometry.

The effects caused by neutron skin are, of course, not limited to $W^\pm$ production but related phenomena are to be expected e.g. in the case of high-p_T photons and charged hadrons which can also be measured at lower center-of-mass energies like those available at the Relativistic Heavy-Ion Collider (RHIC). In the case of lepton–nucleus deeply-inelastic scattering, the neutron skin should affect differently the neutral- and charged-current reactions. Thus, the neutron-skin effect could serve as a handle to study the centrality also at planned deeply-inelastic scattering experiments like the Electron–Ion Collider [58] or LHeC [59].

Acknowledgements

I thank Markus Kortelainen, Sami Räsänen, Kari J. Eskola, Tuomas Lappi and Harri Niemi for discussions.

References

[1] Jan Rak, Michael J. Tannenbaum, High-pT Physics in the Heavy Ion Era, Camb. Monogr. Part. Phys. Nucl. Phys. Cosmol., Cambridge Univ. Press, ISBN 9780521190299, 2013.
[2] Wojciech Florkowski, Phenomenology of Ultra-Relativistic Heavy-Ion Collisions, World Scientific, ISBN 978-981-4280-66-2, 2010.
[3] B. Abelev, et al., ALICE Collaboration, Phys. Rev. C 88 (4) (2013) 044909, arXiv:1301.4361 [nucl-ex].
[4] J. Adam, et al., ALICE Collaboration, arXiv:1412.6828 [nucl-ex].
[5] S. Chatrchyan, et al., CMS Collaboration, Phys. Rev. C 84 (2011) 024906, arXiv:1102.1957 [nucl-ex].
[6] G. Aad, et al., ATLAS Collaboration, arXiv:1405.3936 [hep-ex].
[7] J.Y. Ollitrault, Phys. Rev. D 46 (1992) 229.
[8] B. Alver, G. Roland, Phys. Rev. C 81 (2010) 054905, arXiv:1003.0194 [nucl-th]; B. Alver, G. Roland, Phys. Rev. C 82 (2010) 039903 (Erratum).
[9] S. Chatrchyan, et al., CMS Collaboration, Phys. Rev. C 87 (2013) 014902, arXiv:1204.1409 [nucl-ex].
[10] K. Aamodt, et al., ALICE Collaboration, Phys. Rev. Lett. 105 (2010) 252302, arXiv:1011.3914 [nucl-ex].
[11] B. Abelev, et al., ALICE Collaboration, Phys. Lett. B 719 (2013) 18, arXiv:1205.5761 [nucl-ex].
[12] P. Huovinen, P.V. Ruuskanen, Annu. Rev. Nucl. Part. Sci. 56 (2006) 163, arXiv:nucl-th/0605008.
[13] C. Gale, S. Jeon, B. Schenke, Int. J. Mod. Phys. A 28 (2013) 1340011, arXiv:1301.5893 [nucl-th].
[14] P. Huovinen, Int. J. Mod. Phys. E 22 (2013) 1330029, arXiv:1311.1849 [nucl-th].
[15] S. Chatrchyan, et al., CMS Collaboration, Eur. Phys. J. C 74 (7) (2014) 2951, arXiv:1401.4433 [nucl-ex].
[16] G. Aad, et al., ATLAS Collaboration, arXiv:1412.4092 [hep-ex].
[17] I. Helenius, K.J. Eskola, H. Honkanen, C.A. Salgado, J. High Energy Phys. 1207 (2012) 073, arXiv:1205.5359 [hep-ph].
[18] I. Helenius, K.J. Eskola, H. Paukkunen, J. High Energy Phys. 1305 (2013) 030, arXiv:1302.5580 [hep-ph].
[19] H. Paukkunen, K.J. Eskola, C. Salgado, Nucl. Phys. A 931 (2014) 331, arXiv:1408.4563 [hep-ph].
[20] S. Tarafdar, Z. Citron, A. Milov, arXiv:1405.4555 [nucl-ex].
[21] A. Adare, et al., PHENIX Collaboration, arXiv:1310.4793 [nucl-ex].
[22] G. Martinez-Garcia, arXiv:1408.3108 [hep-ph].
[23] A. Bzdak, V. Skokov, S. Bathe, arXiv:1408.3156 [hep-ph].
[24] M. Alvioli, B.A. Cole, L. Frankfurt, D.V. Perepelitsa, M. Strikman, arXiv:1409.7381 [hep-ph].
[25] D.V. Perepelitsa, P.A. Steinberg, arXiv:1412.0976 [nucl-ex].
[26] N. Armesto, D.C. Gulhan, J.G. Milhano, arXiv:1502.02986 [hep-ph].

[27] C.M. Tarbert, D.P. Watts, D.I. Glazier, P. Aguar, J. Ahrens, J.R.M. Annand, H.J. Arends, R. Beck, et al., Phys. Rev. Lett. 112 (2014) 242502, arXiv:1311.0168 [nucl-ex].
[28] S. Abrahamyan, Z. Ahmed, H. Albataineh, K. Aniol, D.S. Armstrong, W. Armstrong, T. Averett, B. Babineau, et al., Phys. Rev. Lett. 108 (2012) 112502, arXiv:1201.2568 [nucl-ex].
[29] C.J. Horowitz, J. Piekarewicz, Phys. Rev. Lett. 86 (2001) 5647, arXiv:astro-ph/0010227.
[30] R.J. Glauber, G. Matthiae, Nucl. Phys. B 21 (1970) 135.
[31] P. Shukla, arXiv:nucl-th/0112039.
[32] D.G. d'Enterria, arXiv:nucl-ex/0302016.
[33] M.L. Miller, K. Reygers, S.J. Sanders, P. Steinberg, Annu. Rev. Nucl. Part. Sci. 57 (2007) 205, arXiv:nucl-ex/0701025.
[34] M. Arneodo, Phys. Rep. 240 (1994) 301.
[35] N. Armesto, J. Phys. G 32 (2006) R367, arXiv:hep-ph/0604108.
[36] S. Malace, D. Gaskell, D.W. Higinbotham, I. Cloet, arXiv:1405.1270 [nucl-ex].
[37] R. Vogt, Phys. Rev. C 70 (2004) 064902.
[38] G. Antchev, et al., TOTEM Collaboration, Europhys. Lett. 101 (2013) 21004.
[39] A.D. Martin, R.G. Roberts, W.J. Stirling, R.S. Thorne, Eur. Phys. J. C 39 (2005) 155, arXiv:hep-ph/0411040.
[40] R.D. Ball, et al., NNPDF Collaboration, Nucl. Phys. B 877 (2013) 290, arXiv:1308.0598 [hep-ph].
[41] C. Anastasiou, L.J. Dixon, K. Melnikov, F. Petriello, Phys. Rev. D 69 (2004) 094008, arXiv:hep-ph/0312266.
[42] S. Catani, L. Cieri, G. Ferrera, D. de Florian, M. Grazzini, Phys. Rev. Lett. 103 (2009) 082001, arXiv:0903.2120 [hep-ph].
[43] Y. Li, F. Petriello, Phys. Rev. D 86 (2012) 094034, arXiv:1208.5967 [hep-ph].
[44] S. Chatrchyan, et al., CMS Collaboration, Phys. Lett. B 715 (2012) 66, arXiv:1205.6334 [nucl-ex].
[45] ATLAS Collaboration, ATLAS-CONF-2014-023.
[46] CMS Collaboration, CMS-PAS-HIN-13-007.
[47] P. Aurenche, J. Lindfors, Nucl. Phys. B 185 (1981) 274.
[48] H. Baer, M.H. Reno, Phys. Rev. D 43 (1991) 2892.
[49] M. Hirai, S. Kumano, T.-H. Nagai, Phys. Rev. C 76 (2007) 065207, arXiv:0709.3038 [hep-ph].
[50] K.J. Eskola, H. Paukkunen, C.A. Salgado, J. High Energy Phys. 0904 (2009) 065, arXiv:0902.4154 [hep-ph].
[51] D. de Florian, R. Sassot, P. Zurita, M. Stratmann, Phys. Rev. D 85 (2012) 074028, arXiv:1112.6324 [hep-ph].
[52] A. Kusina, K. Kovarik, T. Jezo, D.B. Clark, F.I. Olness, I. Schienbein, J.Y. Yu, arXiv:1408.1114 [hep-ph].
[53] H. Paukkunen, C.A. Salgado, Phys. Rev. Lett. 110 (21) (2013) 212301, arXiv:1302.2001 [hep-ph].
[54] H.L. Lai, M. Guzzi, J. Huston, Z. Li, P.M. Nadolsky, J. Pumplin, C.-P. Yuan, Phys. Rev. D 82 (2010) 074024, arXiv:1007.2241 [hep-ph].
[55] J.M. Campbell, R.K. Ellis, Nucl. Phys. B, Proc. Suppl. 205–206 (2010) 10, arXiv:1007.3492 [hep-ph].
[56] http://mcfm.fnal.gov/.
[57] A. Kusina, T. Stavreva, S. Berge, F.I. Olness, I. Schienbein, K. Kovarik, T. Jezo, J.Y. Yu, et al., Phys. Rev. D 85 (2012) 094028, arXiv:1203.1290 [hep-ph].
[58] E.C. Aschenauer, M.D. Baker, A. Bazilevsky, K. Boyle, S. Belomestnykh, I. Ben-Zvi, S. Brooks, C. Brutus, et al., arXiv:1409.1633 [physics.acc-ph].
[59] J.L. Abelleira Fernandez, et al., LHeC Study Group Collaboration, J. Phys. G 39 (2012) 075001, arXiv:1206.2913 [physics.acc-ph].